

Experiment in Planar Geometry for Shock Ignition Studies

S. D. Baton,¹ M. Koenig,¹ E. Brambrink,¹ H. P. Schlenvoigt,¹ C. Rousseaux,² G. Debras,² S. Laffite,² P. Loiseau,²
F. Philippe,² X. Ribeyre,³ and G. Schurtz³

¹LULI, École Polytechnique, CNRS, CEA, UPMC, route de Saclay, F-91128 Palaiseau, France

²CEA, DAM, DIF, F-91297 Arpajon, France

³Université de Bordeaux–CNRS–CEA, Centre Lasers Intenses et Applications (CELIA), Talence, F-33405, France

(Received 10 July 2011; published 8 May 2012)

The capacity to launch a strong shock wave in a compressed target in the presence of large preplasma has been investigated experimentally and numerically in a planar geometry. The experiment was performed on the LULI 2000 laser facility using one laser beam to compress the target and a second to launch the strong shock simulating the intensity spike in the shock ignition scheme. Thanks to a large set of diagnostics, it has been possible to compare accurately experimental results with 2D numerical simulations. A good agreement has been observed even if a more detailed study of the laser-plasma interaction for the spike is necessary in order to confirm that this scheme is a possible alternative for inertial confinement fusion.

DOI: 10.1103/PhysRevLett.108.195002

PACS numbers: 52.57.–z, 52.38.Bv, 52.50.Lp

Shock ignition (SI), a new approach to inertial confinement fusion (ICF) proposed by Betti *et al.* [1], is being studied as an alternative option for achieving high target gains for inertial fusion energy in the direct drive scheme. This option is now under investigation for the NIF [2], LMJ [3], and HiPER projects [4,5], but preliminary studies are needed to validate the main physics issues. In conventional ICF targets operating under direct or indirect drive, the laser must impart a high velocity to the imploding shell to create the central ignition hot spot at stagnation. In shock ignition, fuel compression and ignition are separated. The idea is to compress the target at low velocity and low isentropic fuel assembly and then to trigger a final “spark” to ignite the compressed fuel by a strong convergent shock launched with a high intensity spike. More precisely, at the end of the shell implosion, final compression is obtained after the outward return shock, coming from the target center, collides with the inward strong shock. The collision of the two shocks results in the formation of a dense, high-pressure region that compresses the hot spot and boosts it up to ignition conditions. In both approaches (classical ICF and SI), control of shock timing and shock coalescence is crucial and has to be demonstrated. It requires experimental studies, as it has been done in the past [6–8] and more recently during the indirect drive ignition campaign at the NIF [9]. Because the implosion velocity is significantly less than the one required for hot spot ignition, considerably more fuel mass can be assembled for the same shell kinetic energy. Thus, like “fast ignition” [10] where the final spark is provided by fast electrons generated by ultra-high intensity laser beam, “shock ignition” has the potential for high gains at low drive energy. The power required to launch the ignition shock lies in the 200–300 TW range. Although this power has already been achieved on NIF [11], the associated damage to focusing optics will be a

challenge at the much higher repetition rate planned for future facilities such as HIPER or inertial fusion energy reactors.

As shock ignition is a new scheme, more and more numerical simulations [1–3,12,13] were widely performed recently. However, only very few experiments have been conducted, in particular, to study, at the same time, the laser-plasma interaction and the shock propagation. A recent experiment performed at the OMEGA laser facility [14] has demonstrated that a properly timed final shock enhances the neutron yield by a factor of 4.

Main issues in the shock ignition context focus on the capacity to launch a high-pressure shock in large coronal plasma and on laser-plasma instabilities (LPI) (stimulated Brillouin and Raman scatterings, SBS and SRS, respectively, two-plasmon decay, TPD) which lead to detrimental effects at high laser intensities ($> 10^{15}$ W/cm²). These effects are essentially energy losses for SBS and SRS and fast electron production for SRS and TPD, leading to fuel preheat. Nevertheless, it is important to note that in the SI scheme these suprathermal electrons are generated in the late phase of implosion where they could be absorbed by the dense imploding shell, thus enhancing shock drive performance [2,15,16].

The experiment, performed at LULI in a planar geometry, addressed these issues: the level of parametric instabilities and a complete description and measurement of the spike shock. The large number of diagnostics turned out to be particularly useful for accurate comparison with numerical simulations and to constraint them, giving confidence in more complex cases where the implementation of diagnostics is more difficult. The experiment was performed at the LULI2000 laser facility with two kJ ns beams almost collinearly. A first beam, denoted as the compression beam, generates both the first shock into the target and

the large coronal plasma; the second one corresponds to the spike beam. The two beams have the same laser characteristics, i.e., 2 ns square pulse duration at 2ω ($0.53 \mu\text{m}$). They are focused with $f/8$ lenses but with two different focal spots in order to reach higher intensities for the spike: $400 \mu\text{m}$ top hat diameter (by using hybrid phase plate) for the compression beam and $100 \mu\text{m}$ diameter for the spike yielding estimated intensities $\sim 7 \times 10^{13} \text{ W/cm}^2$ and up to 10^{15} W/cm^2 , respectively. The spike beam is delayed regarding to the compression beam, from 1 to 2 ns, in order to study the influence of laser-plasma interaction on the coalescence shocks with respect to the delay. The referenced time (t_0) corresponds to the start of the compression beam.

The target was designed with the help of 1D numerical simulations performed with the CHIC code [17]. A schematic drawing of the target is presented in the inset of Fig. 1. It consists of a $50 \mu\text{m}$ plastic (CH) ablator (on the laser side) to absorb the incident laser and to reduce the x-ray production that might preheat the target. Adjoined CH, a $10 \mu\text{m}$ Ti layer blocks x rays from the front side of the plasma but it is also used as a fluorescence layer to diagnose fast electrons via $K\alpha$ emission. The third part of the target consists of a $250 \mu\text{m}$ α -quartz window to observe the shock velocity histories. In order to minimize ghost reflections, the free surface of the quartz is antireflection coated.

A large set of diagnostics has been implemented to estimate, simultaneously, the backscattered energy of the spike (time-resolved reflectivities for SRS and SBS and time-resolved spectrum for SBS only), the time-resolved shock velocities from VISAR (velocity interferometer system for any reflector) [18] and time-resolved self-emission. A Bragg crystal spectrometer used in a von Hamos configuration has been implemented to record the Ti – $K\alpha$ emission generated by fast electrons. In order to get an absolute timing for accurate comparison between experiment and simulations, an optical fiducial synchronized with the laser beam has been added on two streak cameras. Two VISARs with different velocity sensitivities have been used to discriminate the 2π phase-shift ambiguity of the discontinuity of the shock velocity at Ti-quartz interface.

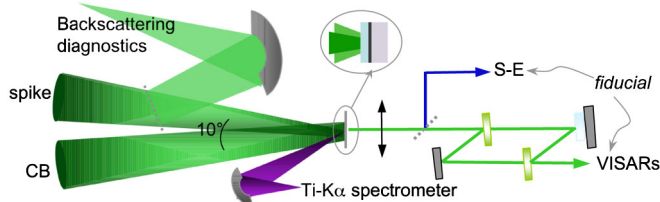


FIG. 1 (color online). Experimental setup. CB corresponds to the compression beam, and S-E to the self-emission diagnostic. A schematic drawing of the target is represented in the circle. The corresponding layer thicknesses are $50 \mu\text{m}$ for CH, $10 \mu\text{m}$ for Ti, and $250 \mu\text{m}$ for SiO_2 .

Etalons of 2.06 and 0.86 mm have been used, giving velocity sensitivities of 15.66 and $37.51 \mu\text{m/ns/fringe}$, respectively. The self-emission from the shock front is detected with a streak camera imaging the rear side of the target coupled with a bandpass filter at $450 \text{ nm} \pm 20 \text{ nm}$. Figure 1 shows a schematic setup with the implemented diagnostics.

As previously mentioned, the parametric instabilities driven by the spike as it propagates through the corona have been analyzed in this experiment. Time-resolved SBS and SRS reflectivities have been measured within the focalization cone ($f/8$) for each shot. Figure 2 represents the reflectivities as a function of the delay between the two beams.

Figure 2 shows that the SBS reflectivities are confined between 7% and 11%, while the SRS reflectivities are below 5%, giving a total reflectivity between 10% and 15%. The total reflectivity has small variations with respect to the pulse delay, and thus to the plasma density scale length. If we consider the numerical simulations performed with the 2D hydrodynamics code FCI2 [19], we can obtain the evolution of electron density during the spike interaction. In particular, the simulation shows a steepening of the density profile at the quarter critical density, which is important for the TPD instability: the density scale length is reduced from $200 \mu\text{m}$ at the beginning of the spike to $10\text{--}20 \mu\text{m}$ at the end. These relatively low reflectivities highlight the complexity of the interaction, particularly the laser-plasma coupling which is very sensitive to the non-linear effects. However, this study is beyond the scope of the present Letter.

A typical VISAR image, recorded for a 1.7 ns delay between the two beams, is displayed in Fig. 3; the time goes down and we can see the fiducial on the right. Three characteristic events are observable: (A) corresponds to the compression shock breakout at the Ti- SiO_2 interface and (B) to the coalescence with the strong shock launched by

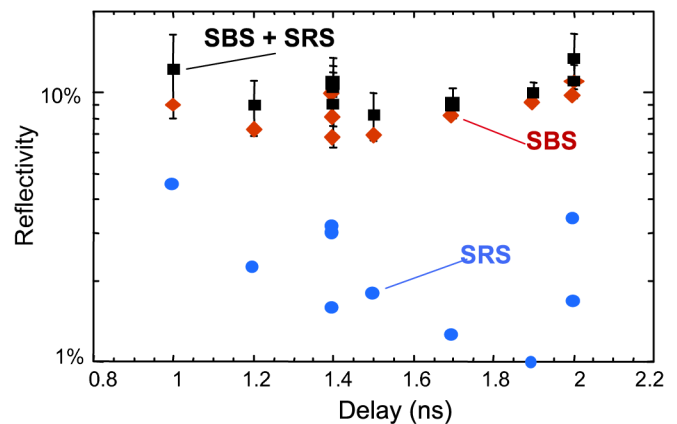


FIG. 2 (color online). Reflectivities in percent of the spike beam within the focalization cone as a function of the delay between the two beams; diamond for SBS, dot for SRS, and square for total reflectivity.

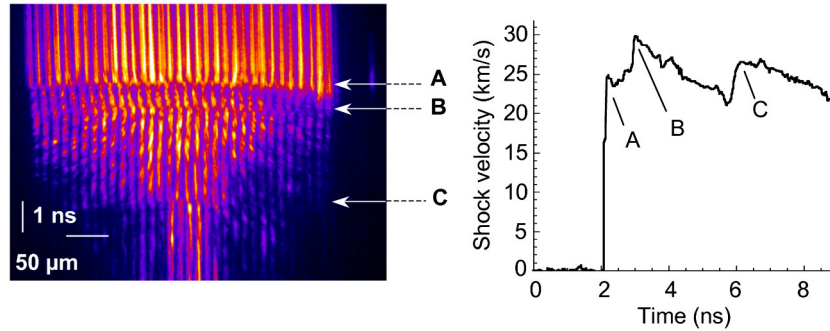


FIG. 3 (color online). VISAR image recorded for a 1.7 ns delay between the two beams (left) and the corresponding shock velocity profile (right). Time goes down. (A) shock breakout of the first beam, (B) coalescence of the two shocks, (C) coalescence between the shock and the compression wave.

the spike beam. The merged shock propagates faster. The third event (C) is not obvious but it can be interpreted thanks to the simulations as discussed further down. From the VISAR data, it is possible to deduce both pressure and temperature of these different events using tabulated Sesame equation-of-state (EOS) [20] and recent works on quartz material [21,22]. We measure a shock velocity of 25 km/s for the shock breakout (A) and 30 km/s for the shock coalescence (B) corresponding to temperature of (4.9 ± 1) eV and (7.3 ± 1) eV, respectively, according to Sesame EOS and velocity error bars. From SE diagnostic (note shown), temperature after the coalescence can also be deduced experimentally, but only relative to the first shock as we did not perform an absolute calibration of this diagnostic [23]. We found a coalescence temperature of 7.9 eV, in agreement with the value deduced from measured shock velocity. These data have been compared with numerical simulations performed with the FCI2 code. After the shock breakout of the first beam, the simulation predicts a temperature of 5.9 eV and after the coalescence, a temperature of 8.5 eV. These values are within errors of the experimental data.

Concerning the results obtained from the x-ray diagnostic, results are limited to the hot electrons able to reach the Ti layer and to excite $K\alpha$. The $K\alpha$ signal was found to be always below the noise level, which gives an upper limit for the hot electron generation. The spectrometer efficiency and the detector sensitivity were characterized with a calibration shot on Ti using known conversion efficiencies [24]. From the cross section for K -shell ionization of Ti [25], this gives an upper limit of 5×10^{12} for the number of electrons above 60 keV (energy loss in the plastic, ionization energy), corresponding to less than 10^{-4} of the laser energy. This estimation, giving low energy for hot electrons, is consistent with the relatively weak value of SRS reflectivity.

For what concerns the VISAR, the data have been directly compared with the 2D Lagrangian radiation-hydrodynamic simulations from FCI2 code. So, the 2D effects arising from the small focal spot size of the spike

beam have been carefully considered. In order to take into account as best as possible the experimental conditions, shots with only one beam (either the compression beam or the spike beam) have been performed. These data from the VISAR and the SE diagnostics obtained with good spatial and temporal resolutions have been used to deduce a realistic spatial distribution in energy. This input parameter, as well as the actual temporal pulse profile, are useful to constraint the simulations. Moreover, the energy loss due to backscattering instabilities is also taken into account.

Figure 4 shows the pressure map as a function of time and space obtained from the 2D simulations for a 1.7 ns delay, corresponding to the data presenting in Fig. 3. The first shock can be followed from the top side ($P \approx 10$ Mbars) until it breaks out in the quartz. Above 1 Mbar pressure, the shock becomes reflecting and thus observable by the VISAR. This is the first event (A). The second shock ($P \approx 40$ Mbars in CH) can be followed too, but only when it catches up with the first shock. This is the second event (B). The pressure of the spike is found to be

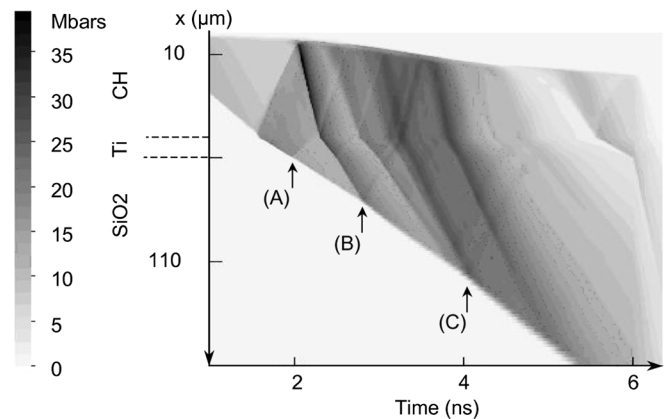


FIG. 4. Pressure (Mbars) as a function of time (in ns) and space (in μm) (Lagrangian coordinates). The three events, shock breakout (A) coalescence of the two shocks (B), and coalescence with the compression wave (C) are observable. Laser beams irradiate the target on the top side of the figure.

TABLE I. Comparison of data obtained from experiment and 2D hydrodynamic code for the shock breakout of the first beam (A) and for the coalescence (B). The delay between the two beams is 1.7 ns. t_0 corresponds to the beginning of the compression beam.

	Time/ t_0 experiment (ns)	Time/ t_0 hydrodynamic code (ns)	Speed experiment (km/s)	Speed hydrodynamic code (km/s)
(A)	2.08 ± 0.05	2.0	25 ± 2	25
(B)	2.9 ± 0.1	2.8	30 ± 2	31

lower than the pressure ablation given by the usual formula [26], which considers the absorbed energy; indeed, our simulations provide a total absorption of the spike of 60%–65%. This highlights the laser-plasma coupling efficiency. The third event (C) occurs when the shock wave is caught up with a compression wave generated in CH after the end of the first pulse while the spike power is still maintained. Indeed, the drop of the first pulse generates an inward rarefaction wave, which propagates behind the first shock. Behind this rarefaction wave, and because the spike still continues, compression waves are launched. Some of them are accelerated by rarefaction waves coming outward from inside the target. They propagate inside the materials and, finally, catch up with the shock. The third event (C) observed in the experiment is the coalescence of one of these compression waves and the shock wave.

Table I summarizes these results for a delay between the two beams of 1.7 ns, corresponding to the Fig. 3. Table I shows a good agreement concerning the time of the breakout shock and the coalescence, as well as for the velocity of these two events. The sensitivity of the numerical results with the incident energy has been considered by taking into account a variation of $\pm 15\%$ of the spike energy (the maximal measured value of scattering losses). The coalescence time is modified within ± 100 ps, which is of the order of the experimental error bars.

It is also then interesting to report on the other shots for which the time delay between the two beams has been systematically varied. The results summarized on Fig. 5,

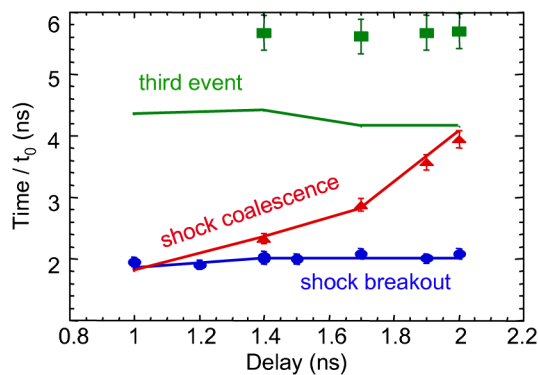


FIG. 5 (color online). Times relative to t_0 (beginning of the compression beam) of the three events as a function of the delay between the two beams obtained in experiment (solid marks) and from 2D simulations (lines).

are plotted together with the numerical predictions. Let us point out the following remarks. First, the trends for the three events are similar both in experiment and simulations. Second, the shock breakout timing (A) is constant for this range of delay, from 1 to 2 ns. As expected, the first shock is not impacted by the interaction of the spike beam. For short delays, the shock coalescence happens before the shock breakout, meaning that the coalescence occurs in the CH or Ti layer, which is not visible from the diagnostics. As the time delay between the two beams increases, the coalescence time occurs much later. This would mean that the velocity of the spike shock decreases with the delay, i.e., as a function of interaction conditions, and/or the velocity of the spike shock decays more rapidly than the first shock velocity. This is in qualitative agreement with the shock geometry: contrary to the first beam focused with a large focal spot giving a planar shock, the second one, due to the small focal spot is sensitive to the 2D effects. It leads to a spherical shock, where energy spreads rapidly inside dense matter, involving deceleration. The third event, the coalescence between compression and shock waves, is mainly correlated to the first beam, so it becomes nearly insensitive to the delay. Figure 5 shows that our experimental data and simulations correctly reproduce this trend. However, a significant discrepancy for the absolute timing is observed. Note that this third event depends on the spike pulse duration, which is here 2 ns. Indeed, according to calculations, the spike pulse duration has been varied and it appears that the third event does not occur for duration less than 500 ps, which is about the duration considered in the shock ignition design for NIF or LMJ [2,3]. Furthermore, the total time width of all compression waves, which finally catch up with the first two shocks, is large (~ 1.5 ns), giving the coalescence time difficult to measure. This third event is specific to this experiment and does not occur in shock ignition target.

In conclusion, the capacity of launching a strong shock wave in a compressed target in the presence of a large preplasma has been demonstrated in planar geometry. An accurate comparison between experimental results and 2D numerical simulations has been possible thanks to a lot of shots by varying the delay between the two beams. Backscattered energy due to SBS and SRS has been measured, yielding a moderate reflectivity less than 15%. The measured shock breakout and coalescence times agree with simulations within experimental accuracy, confirming that laser coupling for shock wave generation at intensities

relevant to shock ignition (10^{15} W/cm²) is appropriately predicted by simulations. Nevertheless, a special effort to diagnose more precisely the laser-plasma interaction for the high intensity beam as well as a full study on the fast electron generation should be planned in future experiment in order to confirm that shock ignition is a possible ICF alternative scheme.

We acknowledge W. Theobald for fruitful discussions.

-
- [1] R. Betti, C.D. Zhou, K.S. Anderson, L.J. Perkins, W. Theobald, and A.A. Solodov, *Phys. Rev. Lett.* **98**, 155001 (2007).
- [2] L.J. Perkins, R. Betti, K.N. LaFortune, and W.H. Williams, *Phys. Rev. Lett.* **103**, 045004 (2009).
- [3] B. Canaud and M. Temporal, *New J. Phys.* **12**, 043037 (2010).
- [4] X. Ribeyre, G. Schurtz, M. Lafon, S. Galera, and S. Weber, *Plasma Phys. Controlled Fusion* **51**, 015013 (2009).
- [5] S. Atzeni, *Plasma Phys. Controlled Fusion* **51**, 124029 (2009).
- [6] A. Kritcher *et al.*, *Science* **322**, 69 (2008).
- [7] H.F. Robey, T.R. Boehly, R.E. Olson, A. Nikroo, P.M. Celliers, O.L. Landen, and D.D. Meyerhofer, *Phys. Plasmas* **17**, 012703 (2010).
- [8] T.R. Boehly, V.N. Goncharov, W. Seka, M.A. Barrios, P.M. Celliers, D.G. Hicks, G.W. Collins, S.X. Hu, J.A. Marozas, and D.D. Meyerhofer, *Phys. Rev. Lett.* **106**, 195005 (2011).
- [9] O.L. Landen *et al.*, *Phys. Plasmas* **18**, 051002 (2011).
- [10] M. Tabak, J. Hammer, M.E. Glinsky, W.L. Kruer, S.C. Wilks, J. Woodworth, E.M. Campbell, M.D. Perry, and R.J. Mason, *Phys. Plasmas* **1**, 1626 (1994).
- [11] S.H. Glenzer *et al.*, *Phys. Rev. Lett.* **106**, 085004 (2011).
- [12] X. Ribeyre, V.T. Tikhonchuk, J. Breil, M. Lafon, and E. Le Bel, *Phys. Plasmas* **18**, 102702 (2011).
- [13] M. Lafon, X. Ribeyre, and G. Schurtz, *Phys. Plasmas* **17**, 052704 (2010).
- [14] W. Theobald *et al.*, *Phys. Plasmas* **15**, 056306 (2008).
- [15] R. Betti *et al.*, *J. Phys. Conf. Ser.* **112**, 022024 (2008).
- [16] O. Klimo, S. Weber, V.T. Tikhonchuk, and J. Limpouch, *Plasma Phys. Controlled Fusion* **52**, 055013 (2010).
- [17] P.-H. Maire, R. Abgrall, J. Breil, and J. Ovidia, *SIAM J. Sci. Comput.* **29**, 1781 (2007).
- [18] P.M. Celliers, D.K. Bradley, G.W. Collins, D.G. Hicks, T.R. Boehly, and W.J. Armstrong, *Rev. Sci. Instrum.* **75**, 4916 (2004).
- [19] D. Besnard, G. Bonnaud, and G. Schurtz, *La Fusion Thermonucléaire Par Laser*, edited by R. Dautray and J.P. Watteau (Eyrolles, Paris 1993), Part 3, Vol. 2, p. 1117.
- [20] See National Technical Information Service Document No. DE94011699 (J.D. Johnson, Los Alamos National Laboratory Report No. LA-UR-94-1451, 1994). Copies may be ordered from the National Technical Information Service, Springfield, Report No. VA 22161.
- [21] D.G. Hicks, T.R. Boehly, J.H. Eggert, J.E. Miller, P.M. Celliers, and G.W. Collins, *Phys. Rev. Lett.* **97**, 025502 (2006).
- [22] M.D. Knudson and M.P. Desjarlais, *Phys. Rev. Lett.* **103**, 225501 (2009).
- [23] J.E. Miller, T.R. Boehly, A. Melchior, D.D. Meyerhofer, P.M. Celliers, J.H. Eggert, D.G. Hicks, C.M. Sorce, J.A. Oertel, and P.M. Emmel, *Rev. Sci. Instrum.* **78**, 034903 (2007).
- [24] D.L. Matthews, E.M. Campbell, N.M. Ceglio, G. Hermes, R. Kauffman, L. Koppel, R. Lee, K. Manes, V. Rupert, V.W. Slivinsky, R. Turner, and F. Ze, *J. Appl. Phys.* **54**, 4260 (1983).
- [25] F.Q. He, X.F. Peng, X.G. Long, Z.M. Luo, and Z. An, *Nucl. Instrum. Methods Phys. Res., Sect. B* **129**, 445 (1997).
- [26] J. Lindl, *Phys. Plasmas* **2**, 3933 (1995).